Computers and Mathematics with Applications 61 (2011) 3668–3677

Contents lists available at ScienceDirect

Computers and Mathematics with Applications

journal homepage: www.elsevier.com/locate/camwa

Numerical investigation of the interactions between solitary waves and pile breakwaters using BGK-based methods

Hongwei Liu [a,*], Mohamed S. Ghidaoui [a], Zhenhua Huang [b], Zhida Yuan [b], Jun Wang [b]

[a] Department of Civil and Environmental Engineering, The Hong Kong University of Science and Technology, Clear Water Bay, Kowloon, Hong Kong

[b] School of Civil and Environmental Engineering, Nanyang Technological University, 50 Nanyang Avenue, Singapore

ARTICLE INFO

Article history:
Received 14 October 2009
Received in revised form 15 March 2010
Accepted 9 June 2010

Keywords:
Shallow water equations
BGK-based methods
Tsunami waves
Pile breakwaters

ABSTRACT

The interactions between a solitary wave, which can be used to model a leading tsunami wave, and a pile breakwater made of circular cylinders are numerically investigated. We use the depth-averaged shallow water equations, which are solved by the finite volume method based on the Bhatnagar–Gross–Krook (BGK) model. The numerical results are compared with the experimental data, which yields very good agreement between them when the ratio of wave height to water depth is small (<0.25). As this ratio exceeds the value of 0.25, the larger the ratio is, the bigger deviation of numerical results from experimental data is observed, the possible reasons for this observation are discussed. Both numerical and experimental results indicate that the transmission of the solitary wave decreases and the reflection of the wave increases with reducing gaps between the adjacent cylinders, and that both transmission and reflection coefficients are not very sensitive to the variation in wave height.

1. Introduction

Tsunami is a series of very long gravity waves generated by either mighty underwater earthquakes or landslides. Tsunami waves in deep oceans typically have heights of less than half meter, but can travel at a speed more than 500 km per hour. When tsunami waves travel into shallow water, shoaling effects may result in very large waves and tremendous breaking activities near-shore, causing significant damage to coastal structures and human lives. The economic and long-term social impacts of tsunami waves, as shown in the 2004 Indian Ocean tsunami, are usually devastating [1,2].

Tsunami forecast and mitigation have been implemented by many coastal nations after the 2004 Indian Ocean tsunami, for example the efforts in Singapore reported in [3] and in United States shown on the website of the National Oceanic and Atmospheric Administration (NOAA). However, the tsunami early warning systems are effective only when all infrastructures and people in tsunami vulnerable communities are prepared and respond appropriately upon the recognition of a potentially destructive tsunami event, and the coastal areas very close to the epicenter may not have enough time to response to the arrival of tsunami waves. Moreover, some tsunami waves, which might not be strong enough to trigger an early warning system to issue a warning, can still cause damage to the harbor facilities due to ship collisions.

Besides tsunami early warning system, active protecting measures are also necessary to protect the vulnerable coastal areas from the attack of local tsunami waves, and to prevent ships from breaking mooring lines and hitting the port facilities due to the tsunami-induced current. Breakwaters are widely-used structures as part of coastal defence, which can be constructed some distance away from the coast or built with one end linked to the coast. Among various types of

* Corresponding author.
E-mail addresses: hwliu@ust.hk, liuhw_pku@yahoo.com.cn (H. Liu).

0898-1221/$ – see front matter © 2010 Elsevier Ltd. All rights reserved.
doi:10.1016/j.camwa.2010.06.012

Fig. 1. A section of the pile breakwater next to Pasir Panjang, Singapore.

breakwaters, those in the form of rigid, slotted vertical barriers are sometimes preferred to provide economical protection from waves in harbors or marinas [4]. One example is the concrete pile breakwater at Pass Christian, Mississippi, which consists of 1.4 m diameter piles with an average spacing of 15.2 cm between piles [5]. Fig. 1 shows another example, i.e. the fixed pile breakwater next to Pasir Panjang, Singapore.

The prediction of the scattering for regular (sinusoidal) waves by a vertical, slotted breakwater is of interest for design purposes. The interactions between regular waves and slotted barriers have been extensively studied by many researchers with experimental, theoretical, and numerical approaches in the past. Wiegel [6] and Hayashi et al. [7] studied the scattering of regular waves by the pile breakwaters, and provided simple expressions for the calculation of the transmission coefficients. Mei et al. [8] analyzed the wave scattering from a slotted barrier by introducing an empirical friction factor. Martin and Dalrymple [9] investigated the scattering of long waves by cylindrical obstacles using matched asymptotic expansions. Kakuno and Liu [10] explored the interactions between water waves and vertical cylinders both theoretically and experimentally. Isaacson et al. [4] constructed a numerical model for the wave interactions with a thin vertical slotted barrier extending from the water surface to certain distance above the seabed, which was assessed by their laboratory tests. In [11], Huang experimentally studied the wave scattering by a slotted barrier in the presence of water current. Later Huang and Ghidaoui [12] proposed a simple model to account for the effects of current on the wave scattering by slotted breakwaters.

Solitary wave has been employed in many related studies to model the leading tsunami wave because the former can represent many important properties of the latter [13]. The interactions between solitary waves and impermeable coastal structures have been studied by many researchers in the past. Seabra-Santos [14] studied the transformation of a solitary wave over a shelf or an isolated obstacle and proposed a numerical model with experimental validation for such problems. Losada et al. [15] experimentally studied the scattering of non-breaking solitary waves when encountering an abrupt discontinuity in depth. Grillis et al. [16] investigated the characteristics of solitary wave breaking induced by emerged and submerged breakwaters by both experiments and computations based on a potential model. Tang & Chang [17], Chang et al. [18] and Huang & Dong [19] investigated the interactions between solitary waves and submerged structures. Liu & Cheng [20] and Lin [13] numerically investigated the evolution of solitary wave over a shelf and rectangular obstacles respectively with the same numerical model. Zhao et al. [21] and Ning et al. [22] numerically studied the interactions between solitary waves and surface-piercing circular cylinders by solving the Boussinesq-type equations.

The nonlinear depth-averaged shallow water equations are often employed in the numerical simulations of the propagation of tsunami waves [23]. However, in the literature survey on the interactions between solitary waves (leading tsunami waves) and slotted breakwaters, the authors could not find the previous research work in which the depth-averaged shallow water equations were used to investigate such problems. The present study is intended to fill this gap to some extent. In [24], Huang et al. have experimentally studied the interactions between solitary waves and pile breakwaters in order to understand the effectiveness of this type of breakwaters in tsunami hazard control. The experimental results have been analyzed by a method based on long wave approximations in [25]. The present work is to investigate the same problem as [24] by numerically solving the shallow water equations and reveal the limitation of the governing equations for this problem by comparing our numerical predictions with the experimental data.

We model in this study the interactions of solitary waves and pile breakwaters by the shallow water equations, the filtering operation is applied to the governing equations and the well-known Smagorinsky model [26] for the subgrid-scale stress is employed to present a large eddy simulation (LES). The filtered shallow water equations are numerically solved by the BGK-based finite volume method [27,28]. In this method, the fluxes for the mass and momentum across the surface of control volume are evaluated from the solution of the BGK equation. One of the distinguished features for the BGK-based method is that it does not require the operator splitting of the advection and diffusion (both molecular and turbulent) terms, which may be problematic in some circumstances, see for example [29,30]. Detailed derivation and various validation of the BGK-based scheme for shallow water flows can be found in [27,31].

In the rest of this paper, the problem description and numerical methodology are presented in Section 2. In Section 3, the numerical results are shown and compared with the experimental data. Finally, main conclusions are summarized in Section 4.

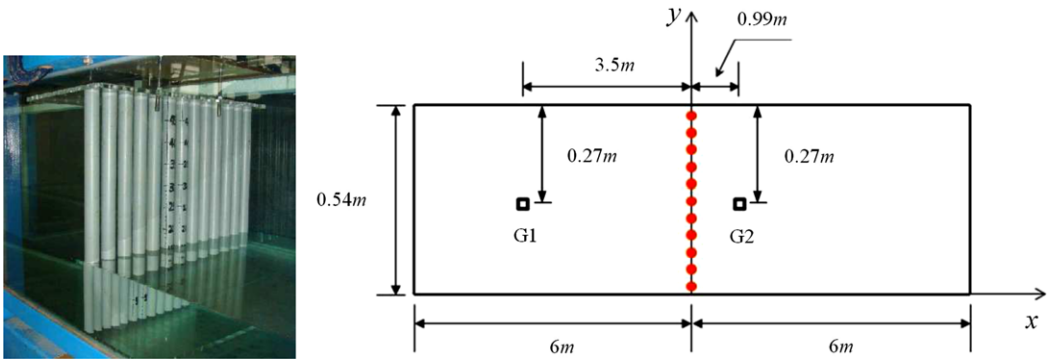

Fig. 2. A view of the pile breakwater used in [24] (left) and the schematic of the computational setup (right).

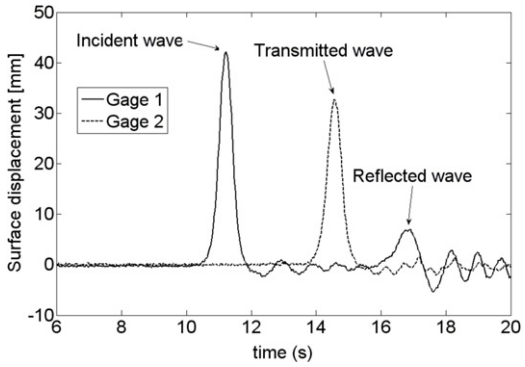

Fig. 3. Measured incident, reflected and transmitted waves in the experiment [24].

2. Problem setup and numerical methodology

Fig. 2 shows a view of one pile breakwater used in the experiment by Huang et al. [24] and the schematic of our computational setup. The wave flume used in the experiment is 32 m long and 54 cm wide. Installed at one end of the wave flume is a piston-type wave generator, which is used to generate the solitary waves. Two Ultrasonic wave gages (General Acoustics) are used to record the surface elevations of incident, reflected and transmitted waves before and behind the breakwater. Referring to Fig. 2, in the experiment the incident and reflected waves are measured at $G1(x = -3.5\text{ m},\ y = 0.27\text{ m})$ point, and the transmitted wave is measured at $G2(x = 0.99\text{ m},\ y = 0.27\text{ m})$ point. Fig. 3 shows a sample of measured incident, reflected, and transmitted solitary waves. It can be seen that there is always an undulating tail behind the solitary wave generated in wave flume. Pile breakwaters consist of an array of circular cylinders of diameter $d = 3$ cm, which are lined up along the y-axis. Two pile breakwater models are used in the experiments, with the center-to-center distance S between two adjacent cylinders being $S = 4.2$ cm (setting 13 cylinders along the cross section of wave flume) and $S = 3.64$ cm (setting 15 cylinders along the cross section of wave flume), respectively. In [24], two undisturbed water depths (15 and 20 cm) are studied, and the height of solitary wave varies from 2 to 10 cm.

In our numerical simulations, the width of the computational domain is the same as that of the experimental wave flume, but the length is chosen to be 12 m to save the computational cost, see Fig. 2. We consider a solitary wave passing through the breakwaters at $x = 0$ from the left to the right. The initial wave shape and velocity are specified by the first-order solitary wave theory [32],

$$\eta(x) = H\text{sech}^2\left[\sqrt{\frac{3H}{4D^3}}(x - X_0)\right], \tag{1}$$

$$u(x) = \eta(x)\sqrt{\frac{g}{D}}, \tag{2}$$

where $\eta(x)$ is the initial free surface displacement and D is the undisturbed water depth, the total water depth h is obtained by $h = D + \eta$; H is the wave height of a solitary wave and g is the gravitational acceleration; X_0 is the position of the initial wave crest, which is set as $X_0 = -3$ m in all our simulations.

We use the depth-averaged shallow water equations to model the interactions of solitary waves and pile breakwaters. It is well known that a solitary wave propagating into still water with constant depth under shallow water equations will

ultimately develop into a vertical leading face and breaking [33,34]. This is due to the lack of dispersive effects for the shallow water equations and can be improved by adding some dispersive terms. However, for many problems, for example the run-up process, the dispersive effects will be small and thus can be neglected [35]. The effects of this ingredient for our problem will be discussed in detail in the next section.

The filtered shallow water equations can be written as [36,37]

$$\frac{\partial \bar{h}}{\partial t} + \frac{\partial (\bar{h}\hat{\bar{u}}_i)}{\partial x_i} = 0, \tag{3}$$

$$\frac{\partial (\bar{h}\hat{\bar{u}}_i)}{\partial t} + \frac{\partial (\bar{h}\hat{\bar{u}}_i\hat{\bar{u}}_j + \delta_{ij} g\bar{h}^2/2)}{\partial x_j} = -g\bar{h}S_i^b + \frac{\partial}{\partial x_j}[\bar{h}(\nu 2\hat{\bar{S}}_{ij} - T_{ij})] - \frac{\bar{\tau}_i^b}{\rho}, \tag{4}$$

where the hat denotes the depth-averaging operator and the bar represents the filtering operator, $i = 1, 2$ and $j = 1, 2$ with 1 indicating x direction and 2 indicating y direction. h is the water depth and u_i is the velocity in x_i direction. S_i^b is the slope of the flow bed along x_i direction. ν is the kinematic viscosity of the fluid, δ_{ij} is the Kronecker delta function. The resolved strain rate tensor $\hat{\bar{S}}_{ij}$ is defined as

$$\hat{\bar{S}}_{ij} = (\partial \hat{\bar{u}}_i/\partial x_j + \partial \hat{\bar{u}}_j/\partial x_i)/2. \tag{5}$$

In Eq. (4), ρ is the fluid density, and $\bar{\tau}_i^b$ is the shear stress at the bed of the flow along x_i direction, which is neglected for our problem since the bottom of wave flume is very smooth. The subgrid-scale tensor T_{ij} represents stresses acting on the vertical plane over the entire depth due to the combined effects of filtering and depth integration [37]. In our numerical simulations, the subgrid-scale stress is modeled by the well-known Smagorinsky eddy viscosity model [26],

$$\nu_t = (C_s\Delta)^2 \left(2\hat{\bar{S}}_{ij}\hat{\bar{S}}_{ij}\right)^{1/2} \tag{6}$$

where ν_t is the eddy viscosity, the Smagorinsky constant C_s is taken as $C_s = 0.065$ [38] and the filter width $\Delta = \sqrt{\Delta x_1 \Delta x_2}$ is adopted.

As pointed out in [37], the filtering and depth-averaging procedures in deriving Eqs. (3) and (4) can be exchanged with the assumption of small surface waves and bed slopes, i.e. $\hat{\bar{\phi}} = \hat{\bar{\phi}}$ for any variable ϕ, see [39,40] for detailed discussions. Therefore the governing Eqs. (3) and (4) can be obtained by two approaches: one is first filtering the Navier–Stokes equations and then averaging the filtered equations over depth, the other is directly filtering the depth-averaged shallow water equations. Interested readers may refer [37] and references therein for more details about the derivation of the filtered shallow water equations.

The filtered shallow water equations are solved by a finite volume method based on the extended BGK equation [27,41]. In this method, the fluxes for the mass and momentum across the surface of the control volume are evaluated from the solution of the BGK equation. The scheme is explicit and second-order in both time and space. A brief description of the BGK-based methods is given in Appendix. Detailed derivation and various validation of the BGK-based schemes for shallow water flows can be found in [27,31]. It should be noted that the BGK-based schemes have been developed and applied to a wide range of flow problems besides the free surface flows, such as the compressible flows [42], near incompressible flows [43], rarefied gas [44] and microscale gas [45] flows. An interested reader may refer to [46] for a general review of the BGK-based schemes.

In our simulations, the free-slip boundary condition is used on the two vertical glass walls of wave flume along x direction, and the no-slip boundary condition is employed on the surfaces of cylinders. The non-reflection boundary condition is implemented at the two ends of computational domain ($x = \pm 6$ m). As shown in Fig. 4, a structured grid with 850×130 elements is used over the whole computational domain, which is refined around circular cylinders. It takes about 7 h for a typical run on our desktop (Intel Core 2 Duo E6750 2.67 GHz). A finer grid with 1700×260 elements gives very similar numerical results, see Fig. 6 for example, where the only visible difference between the numerical results from the coarse and fine grids is around the solitary peak, and the relative difference $|(\eta_{coarse} - \eta_{fine})/\eta_{coarse}|$ is less than one percent, which indicates the convergence of the numerical solution and the adequacy of the grid size used.

3. Numerical results and discussions

In what follows, we use *Hi*, *Hr*, *Ht* to denote the wave heights of the incident, reflected and transmitted waves, respectively. The water depth distribution and stream traces when the incident wave crest is passing through the breakwater are shown in Fig. 5 for a typical case ($S = 4.2$ cm, $D = 15$ cm and $Hi = 2$ cm). From Fig. 5, we can see that the water depth just behind the breakwater is generally smaller than that just in front of the breakwater, which is consistent with the experimental observation [24]. The large scale flow pattern around the cylinders is clearly shown by the stream traces. The recorded surface displacements at G2 point are shown in Fig. 6, where the numerical results from both coarse and fine grids are compared with experimental data and they match well. In this figure, the small tailing waves in the measured data

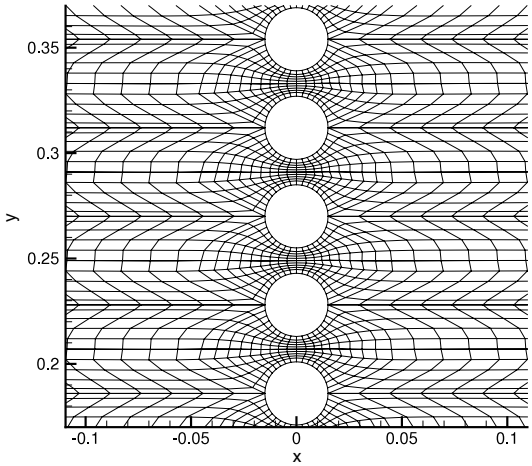

Fig. 4. Computational mesh (850 × 130) around the cylinders for the case with $S = 4.2$ cm.

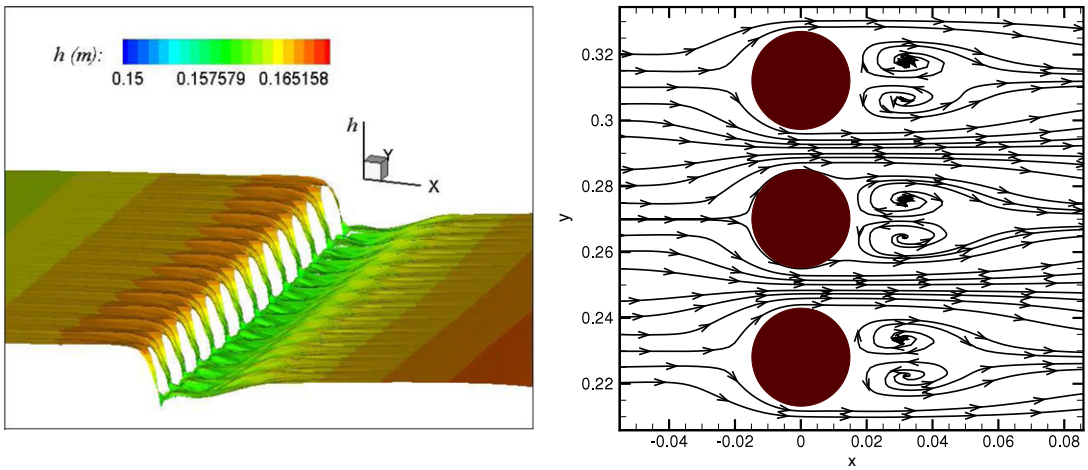

Fig. 5. The distribution of water depth h (left) and stream traces (right) when the incident wave crest is passing through the pile breakwater ($S = 4.2$ cm, $D = 15$ cm, $Hi = 2$ cm).

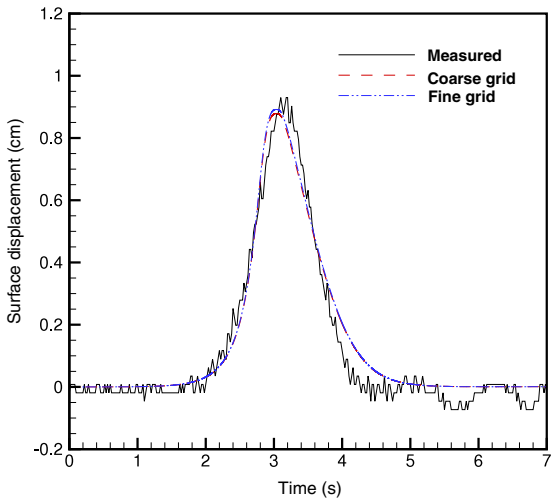

Fig. 6. Recorded surface displacements at G2 point versus time ($S = 4.2$ cm, $D = 15$ cm, $Hi = 1.15$ cm). Coarse grid: 850 × 130; fine grid: 1700 × 260.

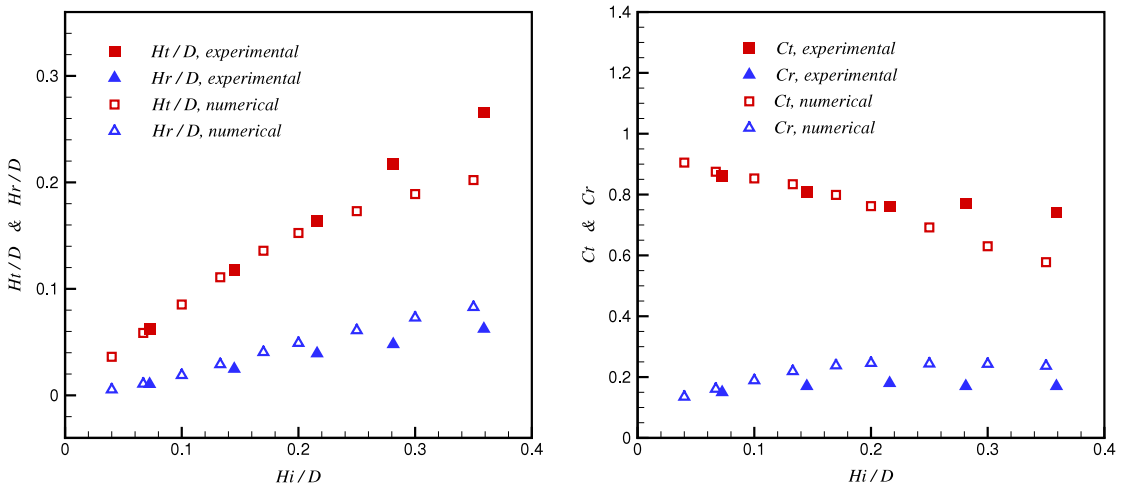

Fig. 7. Numerical results for the case $S = 4.2$ cm, $D = 15$ cm. Ht/D & Hr/D (left), Ct & Cr (right).

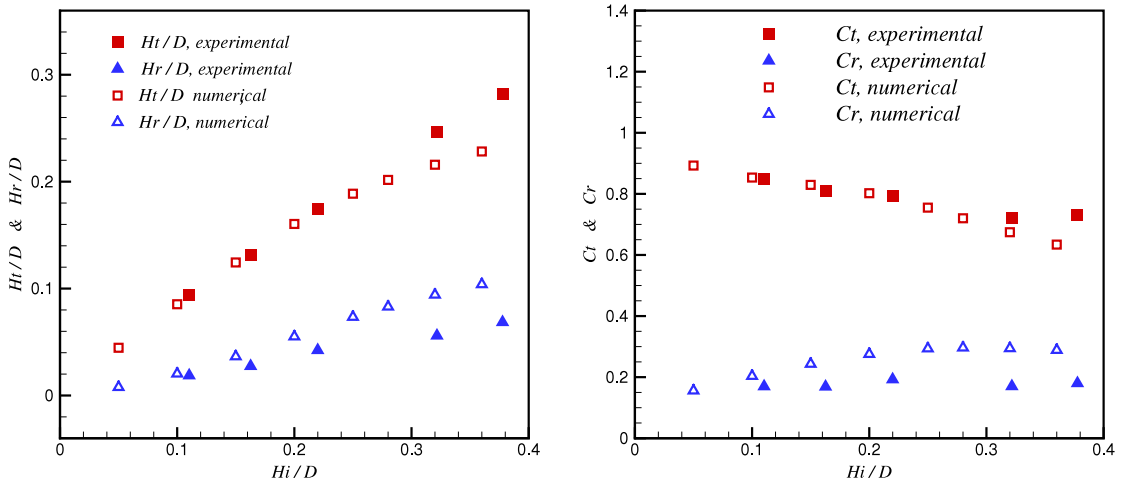

Fig. 8. Numerical results for the case $S = 4.2$ cm, $D = 20$ cm. Ht/D & Hr/D (left), Ct & Cr (right).

(*time* $\in$ [4.5 s, 7 s]) are due to the undulating tail behind the leading solitary wave generated in wave flume, which is absent in the numerical setup of our simulations.

Figs. 7 and 8 show the numerical results for two cases $D = 15$ cm and $D = 20$ cm with $S = 4.2$ cm, respectively. In the figures, the transmitted and reflected wave heights are shown on the left, the transmission and reflection coefficients are given on the right, where the transmission and reflection coefficients are defined as $Ct = Ht/Hi$ and $Cr = Hr/Hi$, respectively. From these figures, we can see that the numerical results agree well with the experimental data when the relative incident wave height (Hi/D) is small (<0.25). As $Hi/D > 0.25$, the larger the ratio is, the bigger the deviation of numerical results from experimental data is. One of the possible reasons for this observation is that the model approximation of shallow water flow loses accuracy as the solitary wave height Hi increases, resulting in reduced wave length L, for constant undisturbed water depth D. For instance, if the solitary wave length L is defined as the distance between the two points where the surface disturbance is 1% of the wave height Hi, then for the case $D = 15$ cm, $Hi/D = 0.25$ we have $L/D \approx 14$, which is already smaller than the widely-accepted limiting value of 20 for L/D where the shallow flow approximation can work well [47].

Another possible reason can be the following. From the characteristic analysis we know that an initial solitary wave will be steepened and cannot keep its wave shape under shallow water equations [33,34]. With the assumption of small ratio of wave height to water depth, the depth-averaged shallow water equations (without bottom slope, viscous and frictional terms) can be linearized into the wave equation, and therefore an initial sinusoidal wave can keep its shape and amplitude during its propagation. For solitary waves, similarly to sinusoidal waves, it has been observed in our numerical simulations that when the relative wave height Hi/D is small, the steepening process performs slowly and therefore affects little to the transmission and reflection coefficients that we are most interested in for the present study. As Hi/D increases, the steepening effect becomes appreciable, hence the deviation of numerical results from experimental data becomes large

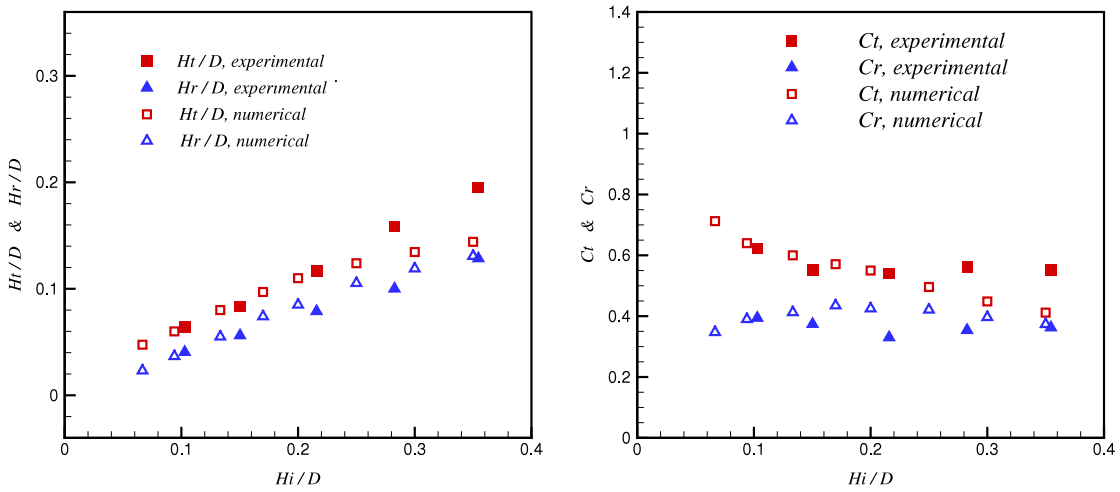

Fig. 9. Numerical results for the case $S = 3.64$ cm, $D = 15$ cm. Ht/D & Hr/D (left), Ct & Cr (right).

and the reliability of numerical results decreases. Finally, very complicated flow structures have been observed as Hi/D increases in the laboratory experiments, for example the air entrainment phenomenon, which cannot be described by the current model. This may also partially cause the large deviation between numerical and experimental results when Hi/D is large.

From Figs. 7 and 8, we can also find that the agreement of transmission coefficient between numerical and experimental results is better than that of reflection coefficient. This may be due to the following reason: for experiment the leading solitary wave is always followed by a series of smaller tail waves, these tail waves should have little effects on the leading transmitted wave, however, they must have some interactions with the leading reflected wave and therefore affect the measured reflection coefficient. In our numerical simulation only a single solitary wave is presented initially because of the difficulty of representing the tail waves, this initial numerical setup is already slightly different from that of the experiment, and such difference of initial data may cause the large deviation for reflection coefficient between numerical and experimental results.

The numerical results for the case $S = 3.64$ cm with $D = 15$ cm are shown in Fig. 9. In this figure, again we see the good agreement between numerical and experimental data when Hi/D is small (<0.25). Comparison between Figs. 7 and 9 indicates that as the gaps between the adjacent cylinders decrease, the transmission coefficient decreases and the reflection coefficient increases. This is consistent with our common expectations. From Figs. 7–9, it can be found that both numerical and experimental results indicate that the transmission and reflection coefficients are not very sensitive to the variation of the relative wave height (Hi/D).

The energy contained per unit wave crest of a solitary wave can be approximately expressed as [48]

$$E = \frac{8\sqrt{3}}{9}\rho g(HD)^{3/2}. \tag{7}$$

From conservation of energy, the loss of solitary wave energy E_L for the problem studied can be computed by $E_L = E_i - E_r - E_t$, where the subscripts i, r, t stand for the incident wave, reflected wave and transmitted wave, respectively. A dimensionless energy loss coefficient C_L can be defined as

$$C_L = E_L/E_0, \quad \text{with } E_0 = 8\sqrt{3}\rho g D^3/9. \tag{8}$$

Fig. 10 gives the energy loss coefficient C_L for the cases $S = 4.2$ cm (left) and $S = 3.64$ cm (right) with $D = 15$ cm. Here again we observe the good agreement between numerical and experimental results when $Hi/D < 0.25$.

4. Conclusions

The interactions between a solitary wave and a slotted breakwater made of circular cylinders are numerically investigated. In the present study we employ the depth-averaged shallow water equations to model the free surface flows, which are solved by the BGK-based finite volume methods. The numerical results are compared with the experimental data, which yields very good agreement between them, especially for the transmission coefficient, when the ratio of wave height to water depth is small ($Hi/D < 0.25$). As this ratio exceeds the value of 0.25, the larger the ratio is, the bigger the deviation of numerical results from experimental data is, and the possible reasons for this observation are discussed. This fact indicates the limitation of the depth-averaged shallow water equations to such type of problems with large relative wave height Hi/D. Both numerical and experimental results indicate that the transmission of the solitary wave decreases

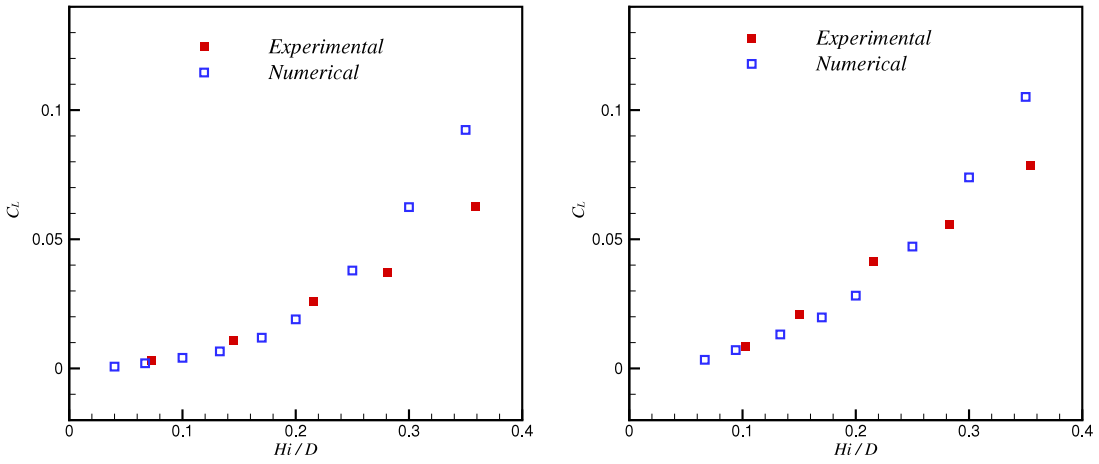

Fig. 10. Energy loss coefficient C_L for the cases $S = 4.2$ cm (left) and $S = 3.64$ cm (right) with $D = 15$ cm.

and the reflection of the wave increases with reducing gaps between the adjacent cylinders, and that both transmission and reflection coefficients are not very sensitive to the variation in wave height.

Acknowledgements

The reported work is partially supported by Research Grant Council, Hong Kong, under the project No. HKUST613306 and partially supported by Nanyang Technological University, Singapore, under the project SUG03/07.

Appendix

The classic depth-averaged shallow water equations can be written in the following compact form,

$$\mathbf{W}_t + \nabla \cdot \mathbf{F} = \mathbf{B}, \tag{A.1}$$

with

$$\mathbf{W} = [h, hu_i]^T, \qquad \mathbf{F}_j = \left[hu_i, hu_iu_j + \frac{1}{2}\delta_{ij}gh^2 - 2\nu hS_{ij}\right]^T,$$

$$\mathbf{B} = \left[0, -ghS_i^b - \frac{\tau_i^b}{\rho}\right]^T, \quad i, j = 1, 2. \tag{A.2}$$

The extended BGK model for the two-dimensional shallow water flows reads [27],

$$\frac{\partial f}{\partial t} + \mathbf{c} \cdot \frac{\partial f}{\partial \mathbf{x}} + \frac{\mathbf{E}}{m} \cdot \frac{\partial f}{\partial \mathbf{c}} = \frac{q - f}{\tau}, \tag{A.3}$$

where f is the particle velocity distribution function, $\mathbf{c}$ is the particle velocity $\mathbf{c} = (c_x, c_y)$, m is the mass of particle and $\mathbf{E}$ the net external force acting on a particle, τ is the relaxation time. The equilibrium distribution function q for shallow water flows is given by

$$q(\mathbf{x}, t, \mathbf{c}) = \frac{1}{\pi g} \exp\left[-\frac{(\mathbf{c} - \mathbf{u})^2}{gh}\right]. \tag{A.4}$$

The BGK equation (A.3) provides a dynamic relation between the equilibrium and non-equilibrium distribution functions at the microscopic level. It is well known that the Navier–Stokes equations can be obtained from the BGK model in conjunction with the Chapman–Enskog expansion [49]. The direct connection between the BGK model and the classical shallow water equations has been established in [27]. In particular, the kinematic viscosity coefficient ν of the fluid can be related to the collision time by

$$\nu = \frac{1}{2}\tau gh. \tag{A.5}$$

In the finite volume framework, an algorithm for the numerical flux $\widetilde{\mathbf{F}}_j$ (both convection and diffusion) across a cell interface is required. Traditional approaches treat the convective and diffusive terms separately, for example upwind techniques

for the former and central difference method for the latter. The BGK-based scheme uses the connection between the BGK equation and the shallow water equations to determine both convective and diffusive flux terms simultaneously, i.e. first the distribution function f at cell interface can be constructed based on the BGK model at the microscopic level, then the macroscopic numerical flux $\widetilde{\mathbf{F}}_j$ for shallow water equations may be obtained by

$$\widetilde{\mathbf{F}}_j = \int \left[c_i, c_i c_j\right]^T f \, \mathrm{d}\mathbf{c}. \tag{A.6}$$

The source term $\mathbf{B}$ in Eq. (A.1) may be treated by the standard operator splitting method [50].

For BGK-based schemes, the construction of distribution function f at cell interface is divided into two steps: (i) data reconstruction and (ii) dynamical evolution based on BGK model. In step (i), the slopes of the conservative variables (components of $\mathbf{W}$) are limited by the van Leer limiter, of course other limiters may be used here. In step (ii), the general analytical solution f of the BGK model (A.3) without forcing term at a fixed position is employed to determine the distribution function at the cell interface. For example, in one-dimensional case with the cell interface $x_{k+1/2}$ we have the following analytical solution of the BGK equation

$$f(x_{k+1/2}, t, c) = \mathrm{e}^{-t/\tau} f_0(x_{k+1/2} - ct, c) + \frac{1}{\tau}\int_0^t q(x', t', c)\mathrm{e}^{(t'-t)/\tau}\mathrm{d}t', \tag{A.7}$$

where f_0 is the initial distribution function at $t = 0$ and $x' = x_{k+1/2} - c(t - t')$. Two unknowns f_0 and q must be specified in Eq. (A.7) in order to obtain the solution $f(x_{k+1/2}, t, c)$. The detailed strategies to address f_0 and q can be found in [46,27,41], which are not repeated here to save space. Once $f(x_{k+1/2}, t, c)$ in Eq. (A.7) is obtained, the numerical flux across the cell interface for the finite volume method can be computed from Eq. (A.6).

For the filtered shallow water equations, if the eddy viscosity turbulence model is used for the subgrid-scale stress, then the filtered Eqs. (3) and (4) are mathematically equivalent to the classical unfiltered shallow water equations by replacing h, u_i and ν by $\bar{h}$, $\tilde{\bar{u}}_i$ and $\nu + \nu_t$, respectively. Thus the BGK-based finite volume method can apply to solve the filtered shallow water equations directly [36,51].

References

[1] V.V. Titov, A.B. Rabinovich, H.O. Mofjeld, R.E. Thomson, F.I. Gonzalez, The global reach of the 26 december 2004 Sumatra Tsunami, Science 309 (2005) 2045–2048.
[2] W.N. Adger, T.P. Hughes, C. Folke, S.R. Carpenter, J. Rockstrom, Social-ecological resilience to coastal disasters, Science 309 (2005) 1036–1039.
[3] Z.H. Huang, T.S. Wu, S.T. Tan, K. Megawatt, F. Shaw, X.Z. Liu, T.C. Pan, Tsunami hazard from the subduction megathrust of the south China sea, part II: hydrodynamic modeling and possible impact on Singapore, J. Asian Earth Sci. 36 (2009) 93–97.
[4] M. Isaacson, S. Premasiri, G. Yang, Wave interactions with vertical slotted barrier, J. Waterway Port Coastal Ocean Eng. 124 (3) (1998) 118–126.
[5] J.B. Herbich, Pile and offshore breakwaters, in: J.B. Herbich (Ed.), in: Handbook of Coastal and Ocean Engineering, vol. 1, Gulf Publishing Company, 1990, pp. 895–920.
[6] R.L. Wiegel, Closely spaced piles as a breakwater, Dock Harbor Authority 42 (491) (1961) 150.
[7] T. Hayashi, T. Kano, M. Shirai, Hydraulic Research on Closely-spaced Pile Breakwaters, in: Proceedings of 10th Coastal Engineering Conference, vol. 2, 1966, pp. 873–884.
[8] C.C. Mei, P.L.-F. Liu, A.T. Ippen, Quadratic head loss and scattering of long waves, J. Waterway Harbour Coastal Eng. Div. 99 (1974) 209–229.
[9] P.A. Martin, R.A. Dalrymple, Scattering of long waves by cylindrical obstacles and gratings using matched asymptotic expansions, J. Fluid Mech. 188 (1988) 465–490.
[10] S. Kakuno, P.-F. Liu, Scattering of water waves by vertical cylinders, J. Waterway Port Coastal Ocean Eng. 119 (3) (1993) 302–322.
[11] Z.H. Huang, An experimental study of wave scattering by a vertical slotted barrier in the presence of a current, Ocean Eng. 24 (2006) 717–723.
[12] Z.H. Huang, M.S. Ghidaoui, A model for the scattering of long waves by slotted breakwaters in the presence of currents, Acta Mech. Sin. 23 (2007) 1–9.
[13] P. Lin, A numerical study of solitary wave interaction with rectangular obstacles, Coastal Eng. 51 (1) (2004) 35–51.
[14] F.J. Seabra-Santos, D.P. Renouard, A.M. Temperville, Numerical and experimental study of the transformation of a solitary wave over a shelf or isolated obstacle, J. Fluid Mech. 176 (1987) 117–134.
[15] M.A. Losada, C. Vidal, R. Medina, Experimental study of the evolution of a solitary wave at an abrupt junction, J. Geophys. Res. 94 (C10) (1989) 14557–14566.
[16] T. Grillis, M.A. Losada, F. Martin, Characteristics of solitary wave breaking induced by breakwaters, J. Waterway Port Coastal Ocean Eng. 120 (1994) 74–92.
[17] C.J. Tang, J.H. Chang, Flow separation during solitary wave passing over submerged obstacle, J. Hydraul. Eng. 124 (1998) 742–749.
[18] K.A. Chang, T.J. Hsu, P.L.-F. Liu, Vortex generation and evolution in water waves propagating over a submerged rectangular obstacle part I, Solitary Waves, Coastal Eng. 44 (1) (2001) 13–36.
[19] C.-J. Huang, C.-M. Dong, On the interaction of a solitary wave and a submerged dike, Coastal Eng. 43 (2001) 265–286.
[20] P.L.-F. Liu, Y. Cheng, A numerical study of the evolution of a solitary wave over a shelf, Phys. Fluids 13 (6) (2001) 1660–1667.
[21] M. Zhao, L. Cheng, B. Teng, Numerical simulation of solitary wave scattering by a circular cylinder array, Ocean Eng. 34 (2007) 489–499.
[22] D.Z. Ning, J. Zang, Q. Liang, P.H. Taylor, A.G.L. Borthwick, Boussinesq cut-cell model for non-linear wave interaction with coastal structures, Int. J. Numer. Meth. Fluids 57 (2008) 1459–1483.
[23] G.R. Gisler, Tsunami simulations, Annu. Rev. Fluid Mech. 40 (2008) 71–90.
[24] Z.H. Huang, J. Wang, L.Y. Koh, An experimental study of interactions of leading tsunami wave with slotted breakwater, in: The 2nd International Symposium for Shallow Flows, Hong Kong, 2008, pp. A0189.
[25] Z.H. Huang, Z.D. Yuan, Transmission of solitary waves through slotted barriers: A laboratory study with analysis by a long wave approximation, J. Hydro-environment Res. 3 (2010) 179–185.
[26] J. Smagorinsky, General circulation experiments with the primitive equations: I. The basic experiment, Mon. Weather Rev. 91 (3) (1963) 99–164.
[27] M.S. Ghidaoui, J.Q. Deng, K. Xu, W.G. Gray, A Boltzmann based model for open channel flows, Int. J. Numer. Methods Fluids 35 (2001) 449–494.
[28] K. Xu, A well-balanced gas-kinetic scheme for the shallow water equations with source terms, J. Comput. Phys. 178 (2002) 533–562.
[29] K.H. Karlsen, K.A. Lie, J.R. Natvig, H.F. Nordhaug, H.K. Dahle, Operator splitting methods for systems of convection–diffusion equations: nonlinear error mechanisms and correction strategies, J. Comput. Phys. 173 (2001) 636–663.

[30] K. Xu, M.L. Mao, L. Tang, A multidimensional gas-kinetic BGK scheme for hypersonic viscous flow, J. Comput. Phys. 203 (2005) 405–421.
[31] M.S. Ghidaoui, J.H. Liang, F.C. Chan, S.Q. Zhang, BGK based finite volume scheme for hydraulic applications, Int. J. Comput. Fluid Dyn. 20 (6) (2006) 439–451.
[32] P. Lin, Numerical Modeling of Water Waves, Taylor & Francis Group, London, 2008.
[33] O. Bhler, A shallow-water model that prevents nonlinear steepening of gravity waves, J. Atmos. Sci. 55 (1998) 2884–2891.
[34] Y. Li, P. Sclavounos, Non-breaking and breaking solitary wave run-up, J. Fluid Mech. 456 (2002) 295–318.
[35] Y. Li, Tsunamis: non-breaking and breaking solitary wave run-up, Technical Report, California Institute of Technology, Pasadena, CA, 2000.
[36] M.S. Ghidaoui, A.A. Kolyshkin, J.H. Liang, F.C. Chan, Q.B. Li, K. Xu, Linear and nonlinear analysis of shallow wakes, J. Fluid Mech. 548 (2006) 309–340.
[37] C. Hinterberger, J. Frohlich, W. Rodi, Three-dimensional and depth-averaged large-eddy simulations of some shallow water flows, J. Hydraul. Eng., ASCE 133 (8) (2007) 857–872.
[38] P. Moin, J. Kim, Numerical investigation of turbulent channel flow, J. Fluid Mech. 118 (1982) 341–377.
[39] C. Hinterberger, J. Frölich, W. Rodi, Depth-averaged large eddy simulation of shallow water flows modelling aspects, in: I.P. Castro, P.E. Hancock (Eds.), Proc., 9th European Turbulence Conf. Advances in Turbulence IX, CIMNE, Barcelona, Spain, 2002, pp. 211–214.
[40] C. Hinterberger, Dreidimensionale und tiefengemittelte large-eddy-simulation von Flachwasserströmungen, Ph.D. Thesis, Univ. of Karlsruhe, Germany, http://www.uvka.de/univerlag/volltexte/2004/25/, 2004.
[41] J.H. Liang, M.S. Ghidaoui, J.Q. Deng, W.G. Gray, A Boltzmann-based finite volume algorithm for surface water flows on cells of arbitrary shapes, J. Hydraul. Res., IAHR 45 (2) (2007) 147–164.
[42] H. Liu, K. Xu, A Runge–Kutta discontinuous Galerkin method for viscous flow equations, J. Comput. Phys. 224 (2007) 1223–1242.
[43] Z.L. Guo, H. Liu, L.S. Luo, K. Xu, A comparative study of the LBM and GKS methods for 2D near incompressible flows, J. Comput. Phys. 227 (2008) 4955–4976.
[44] K. Xu, H. Liu, Multiscale gas-kinetic simulation for continuum and near continuum flows, Phys. Rev. E 75 (2007) 016306.
[45] K. Xu, H. Liu, J.Z. Jiang, Multiple temperature kinetic model for continuum and near continuum flows, Phys. Fluids 19 (2007) 016101.
[46] K. Xu, A gas-kinetic BGK scheme for the Navier–Stokes equations and its connection with artificial dissipation and Godunov method, J. Comput. Phys. 171 (2001) 289–335.
[47] P.S. Eagleson, R.G. Dean, Small amplitude wave theory, in: A.T. Ippen (Ed.), Estuary and Coastline Hydrodynamics, McGraw-Hill, 1966, pp. 1–92.
[48] R.M. Sorensen, Basic Coastal Engineering, Springer, 2006.
[49] W.G. Vincenti, C.H. Kruger, Introduction to Physical Gas Dynamics, Wiley, New York, 1965.
[50] R.J. LeVeque, Numerical Methods for Conservation Laws, Birkhäuser Verlag, Boston, 1992.
[51] H. Liu, M.Y. Lam, M.S. Ghidaoui, Numerical study of temporal shallow mixing layers using BGK-based schemes, Comput. Math. Appl. 59 (7) (2010) 2393–2402.